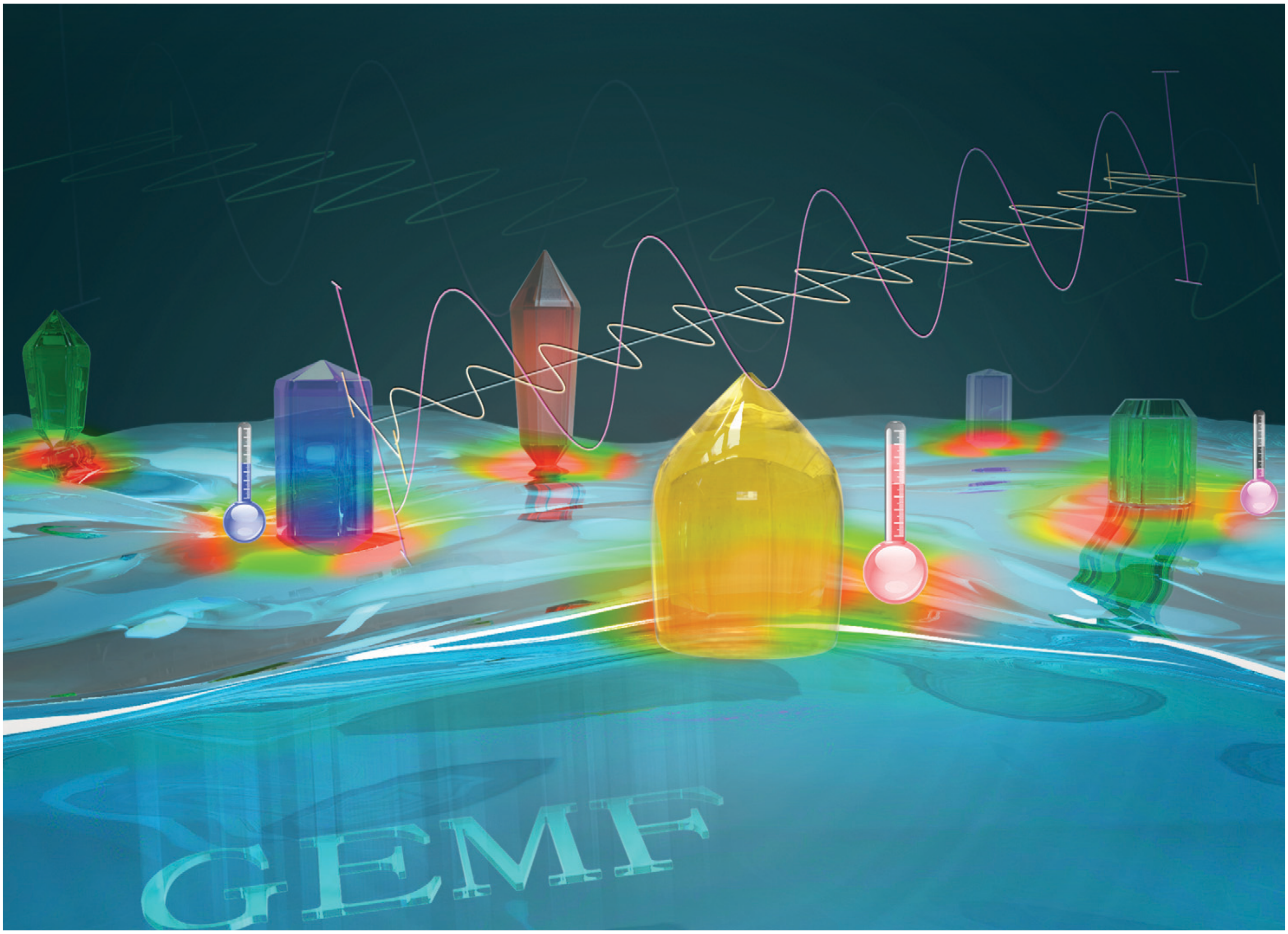

Showcasing research work by Yunzhong Zhu, Shaopeng Lin, Zhihua Liu, Wenjia Wang, Decai Ma* and Biao Wang* from Prof. Biao Wang's group at Sino French Institute of Nuclear Engineering and Technology, Sun Yat-sen University, China.

In situ visualization of the quasi-periodic crystal growth interface fluctuation by growth interface electromotive force spectrum in a Czochralski system

This work uses the growth interface electromotive force (GEMF) to quantify the real-time states of subtle growth rate and temperature fluctuations and depicts the regularities of coupled melt convection and spoke flow pattern, which reveals the convection instability in a melt growth system *in situ*.

As featured in:

See Decai Ma, Biao Wang *et al.*, *CrystEngComm*, 2019, **21**, 1107.

ROYAL SOCIETY OF CHEMISTRY | Celebrating IYPT 2019

rsc.li/crystengcomm

CrystEngComm

PAPER

View Article Online
View Journal | View Issue

Check for updates

Cite this: CrystEngComm, 2019, 21, 1107

In situ visualization of the quasi-periodic crystal growth interface fluctuation by growth interface electromotive force spectrum in a Czochralski system

Yunzhong Zhu, [a] Shaopeng Lin, [a] Zhihua Liu,[b] Wenjia Wang,[b] Decai Ma *[a] and Biao Wang*[ab]

Received 14th November 2018,
Accepted 4th December 2018

DOI: 10.1039/c8ce01949e

rsc.li/crystengcomm

Inhomogeneity and striations stemming from growth interface fluctuation impair the performance of bulk single crystals. Although an enormous number of theoretical and experimental simulations have generalized interface fluctuations, *in situ* detection at high temperatures of the constantly-changing Czochralski (CZ) system is still unattainable. To solve this issue, we used growth interface electromotive force (GEMF) to reveal interface fluctuations and visualize both the corresponding subtle growth rate and temperature fluctuations in a real CZ system. In addition, GEMF could present the regularity of the coupled melt convection as well as predict a gradient surface morphology. Notably, the visualization of the above phenomena is far beyond the capability of current crystal growth sensors. However, based on the GEMF method, significant evidence to reveal convection instability is achieved. More importantly, the high-precision *in situ* GEMF feedback could bridge the quasi-periodic interface fluctuation with convection control approaches and serve as visual guidance for optimization of the growth system, which serves to achieve a striation-free high quality crystal boule.

1. Introduction

Single crystalline materials have supported the development of optic and electronic fields for decades. Moreover, numerous techniques have been investigated to optimize crystal quality. Among all the growth methods, the widely used Czochralski (CZ)[1] system could be essentially generalized as an epitaxial process of a solid-melt interphase (growth interface), which is the core region to determine crystal quality.[2–4] However, it is also a hidden region, since the interface convection and temperature fluctuations are barely observed during growth.[5–8] These fluctuations are mainly driven by three factors: output power, crystal rotation and melt convection.[9] The first two are external factors and depend on the growth system, but the third is an internal factor, which has been widely investigated and even simplified as a typical CZ convection parameter.[10–12] In the CZ melt model, Marangoni and buoyancy flow (natural convection) are driven by temperature differences in the melt, and the Ekman flow (forced convection) derives from the crystal or crucible rotation.[13–19] Inevitably, the competition of natural and forced convection will fluctuate the crystallization process drastically, which is the essential factor for macroscopic defects such as growth striations and component segregation.[16,20,21] Although they are regarded as intrinsic defects and seem unavoidable, methods including microgravity, magnetic field, ultrasound field, accelerated crystal/crucible rotation technique (ACRT) and axial vibrational control (AVC)[22–26] have been tried to settle this issue at the source, namely, suppressing interface fluctuation by manually controlling the flow. The above methods perform well in melt homogenization, but unfortunately, the suppression of melt fluctuation cannot function through the whole growth process. This is due to the constantly-changing melt flow beneath the interface that is extremely sensitive to disturbances and strongly affected by growth condition. Although an enormous number of quasi-steady state simulations have revealed the thermo- and hydrodynamic processes of CZ crystal growth,[2,27,28] the time-dependent fluctuation of practical melt convection is still unpredictable.[29] Thus, without *in situ* feedback of the growth interface, diverse fluctuation suppression methods can hardly perform as expected.

In this study, we visualized the subtle growth rate fluctuations and temperature undulation by growth interface electromotive force (GEMF). In addition, an odd morphology of gradient striations was predicted and validated to

[a] *Sino French Institute of Nuclear Engineering and Technology, Sun Yat-sen University, Zhuhai, 519082, China. E-mail: zhuyzh7@mail.sysu.edu.cn, madecai@mail.sysu.edu.cn*
[b] *School of Physics, Sun Yat-sen University, Guangzhou 510275, China. E-mail: wangbiao@mail.sysu.edu.cn*

demonstrate the outstanding sensitivity and accuracy of the GEMF method. The widely investigated congruent lithium niobate (CLN) single crystal was selected as the study carrier.[30–32] Based on our previous study on the GEMF spectrum and the *in situ* detection of growth striations in CZ systems,[33,34] we tried to reveal interface fluctuations with the aid of the sensitive response of GEMF to crystallization and supercooling phenomena.[35] Since GEMF contains electro-motive force (EMF) generated from the crystallization, transport and segregation of ionic species,[35] the related factors of ion accumulation and component segregation could be revealed. Particularly, in the CZ melt growth system, the above factors are strongly tied to the growth rate and supercooling degree, which could act as visual guidance to reveal interface instability and optimize crystal quality.

2. Material and methods

2.1 Bulk single crystal growth

The CLN raw mixture consists of high purity (99.99%) Li_2CO_3 and Nb_2O_5 in a molar ratio of 0.946. After ball milling and calcining, the CLN polycrystalline powder was melted (above 1240 °C) in a platinum crucible (radius R = 40 mm, height H = 50 mm, melt level h = 35 mm) in a CZ furnace. Before crystal growth, the seed crystal, crucible and thermal insulations were well aligned. The eccentricity of the crystal rotating system was limited to 0.3 mm, which represented the radius difference between the crystal boule and rotation edge. Then, the single crystal was grown along the z-axis [001] in 10 mm radius (r). The pulling and rotation rates, within 1–10 mm h^{-1} and 1–30 rpm, respectively, were chosen to characterize the specific convection and temperature phenomena in the GEMF spectra.

2.2 Temperature measurements

Three thermocouples (T, T', T_1) were added for three specific experiments. As shown in Fig. 1a, T is the conventional measuring point for CZ crystal growth. Another thermocouple T', placed in the melt beside the growth interface, rotates with the boule and records the azimuthal temperature variation simultaneously. When T', T and the melt level are set in a horizontal line, the temperature difference (T_{dif}) between the growth interface and the edge of the melt could be obtained. Therefore, combining with the known growth parameters, the important hydrodynamic parameters, namely, Grashof and Reynolds numbers (Gr and Re, respectively), could be calculated to benefit the numerical simulation study. Gr = $g\beta_T T_{dif} R^3/\nu^2$ and Re = $\omega r^2/\nu$,[36] where g is the gravitational acceleration (9.8 m s^{-2}) and β_T is the volumetric expansion coefficient (1.7 × 10^{-4} K^{-1}). The kinematic viscosity ($\nu = \mu/\rho$) is 1.12 × 10^{-5} m^2 s^{-1}, where μ is the viscosity (4.12 × 10^{-2} kg m^{-1} s^{-1}) and ρ is the density (3.67 × 10^3 kg m^{-3}) of the CLN melt.[37] Then, in our system, since T_{dif} was 27 K and ω was the angular velocity of crystal rotation (rad s^{-1}), Gr was 22 950 and Re at 1, 14, and 30 rpm was 0.93, 13.08 and 28.04, respectively. It should be noted that in growth duration, T_{dif} gradually changed with the melt level and the growing boule, but T' in our study was only measured at the beginning of diameter control. In addition, T_1 was attached to the seed crystal to record the GEMF hysteresis loop. Furthermore, to compare the loops at different pulling rates, the temperature range of T_1 was deliberately limited.

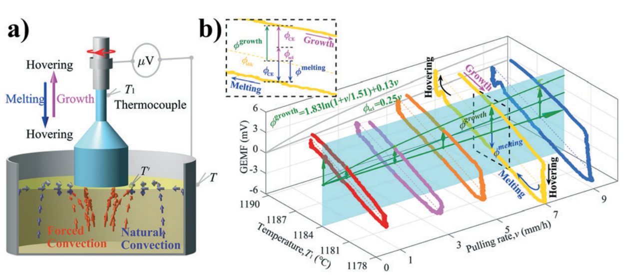

Fig. 1 (a) Schematic of crystal growth system, GEMF data acquisition system and melt convection configuration. (b) The GEMF hysteresis loops, acquired from growth, hovering and melting processes in different growth rates, could fit out the relationships among crystal growth EMF, supercooling EMF and growth rate: $\phi^{growth}(v)$ and $\phi_{scl}(v)$. The inset presents the detailed components of hysteresis potential.

2.3 GEMF hysteresis loops and components

As shown in Fig. 1b, the hysteresis loop refers to the GEMF variation (ϕ_{GE} *vs.* T_1) during the growth, hovering and melting of a growing boule.[34] The obtained hysteresis potential is due to the multicomponent EMFs in GEMF. Specifically, it is composed of thermal EMF and crystallization EMF (ϕ_{CE}), $\phi_{GE} = \phi_{sbk} + \phi_{scl} + \phi_{CE}$. The thermal EMF is considered as a collection of Seebeck EMF (ϕ_{sbk}, relates with the pulling height) and supercooling EMF (ϕ_{scl}). In fact, ϕ_{scl} is also a type of Seebeck potential, but only exists in the growth process and linearly increases with growth rate (v) ($\phi_{scl} = A \times v$, where A is the supercooling coefficient).[38] In addition, ϕ_{CE} comes from the partitioning of opposite ions on both sides of the interface, and shows the opposite behaviour and reverses from crystallization to dissolution.[35] Furthermore, benefitting from the above physical and chemical characteristics of EMFs, a detailed description of the hysteresis potential could be drawn, as shown in the inset of Fig. 1b. Since ϕ_{sbk} is the only remaining EMF in a hovering boule, the connection of both ends of hovering lines could separate the hysteresis potential into growth ($\phi^{growth} = \phi_{CE} + \phi_{scl}$) and melting EMFs ($\phi^{melting} = \phi_{CE}$). Moreover, Aleksandrovskii generalizes the growth interface as a semiconductive model that connects growth rates with the hysteresis potentials;[39] considering the Seebeck effect, the supercooling degree (T_{scl}) is proportional to ϕ_{scl}.[38] Then, the functions of $\phi^{growth}(v)$ and $T_{scl}(v)$ in different growth rates could be obtained as shown in Fig. 1b,[34,38–40]

$$\phi^{growth} = [\phi_0 \ln(1 + v/v_0) + A \times v]/2 \tag{1}$$

$$T_{scl} = A \times v/(\alpha_L - \alpha_S) \tag{2}$$

where ϕ_0 = 3.65 mV, v_0 = 1.51 mm h^{-1} and A = 0.25 mV h mm^{-1} are the fitted system-dependent coefficients in our CZ system; α_L = 0.23 mV K^{-1} and α_S = −0.71 mV K^{-1} are the Seebeck coefficients of the CLN melt and solid, respectively.[34]

2.4 GEMF signal acquisition and processing

In the CZ system, the GEMF spectrum was acquired between the platinum crucible and the pulling rod (as shown in Fig. 1a). The obtained GEMF spectra at different rotation rates are processed *via* fast Fourier transform (FFT) with a Hanning-window. Due to the crystallization and thermal phenomena at the growth interface, the power spectrum of the mean squared amplitude (power as MSA) of the specific GEMF spectrum could present the characteristic peaks of the melt convection and crystal rotation together. Since the Seebeck EMF simply relates with the pulling height, in FFT processing, it appears as an ultra-low frequency with considerable amplitude and should be filtered out from the MSA spectrum. Then, if we extract the characteristic waves from the GEMF, the specific performance of convection and rotation could be investigated. Further analysis and prediction could be verified by the real surface morphology (striations) of the as-grown crystal. In the GEMF data acquisition system, a multimeter (Keithley 2100) was used to capture the electric signal at a sampling rate of 10 S s^{-1} (samples per second). The morphology of the crystal surface was scanned by a high-resolution atomic force microscope (AFM, Asylum Research MFP-3D infinity) with a low noise of 0.15 nm.

3. Results and discussion

The interface is one of the most important aspects of crystal growth, whose temperature variation in the rotation path generates rotation striations directly.[41] In addition, the complex flow pattern in a free melt surface disturbs the stable interface. More importantly, the elusory melt flow fluctuates the growth interface drastically. The rotation-based temperature variation is due to the unavoidable mechanical imbalance and dissymmetric temperature field;[42] the intrinsic azimuthal temperature undulation in the melt surface comes from the "spoke" flow pattern controlled by the coupled Marangoni-buoyancy convection.[14,43] Moreover, the forced convection further complicates the CZ-melt and forms a "cold plume" instability.[10] Clearly, the conventional measuring point beside the high-heat crucible cannot reflect the temperature and convection fluctuations under the growth interface, let alone the camera above the melt and the weight sensor which is not sensitive enough. Our solution depends on the sensitive GEMF spectrum, which takes three cases, namely, low, medium and high crystal rotation rates (1, 14, and 30 rpm) as examples for the following discussion.

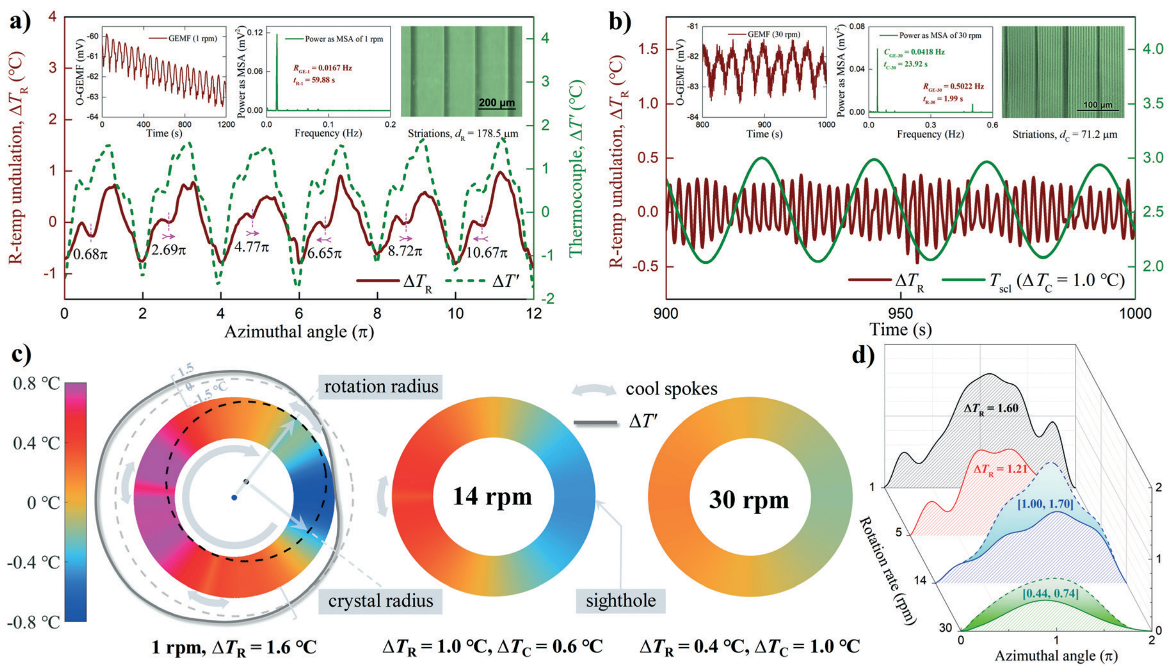

Fig. 2 (a) The rotation-induced azimuthal temperature undulation (R-temp, ΔT_R) at 1 rpm; the dashed line depicts the measured temperature undulation of the thermocouple ($\Delta T'$) rotating with the boule. The displacements of inflection points (pink arrows) are labelled. The insets present the original GEMF (O-GEMF) data, corresponding MSA spectrum and growth (rotation) striations. (b) The R-temp undulation and the convection-induced variation of supercooling degree (T_{scl}) in 30 rpm, the convection-induced temperature undulation (C-temp, ΔT_C) is 1.0 °C. The insets present its O-GEMF, corresponding MSA spectrum and growth (convection and rotation) striations. (c) The pie graphs visualize the spoke flow patterns and azimuthal temperature undulations at low, medium and high rotation rates. The eccentric-disk rotation model is labelled at 1 rpm, the blue and black dots represent the centres of crystal rotation and boule, respectively; the black dashed circle represents the eccentric rotating growth interface; the grey loop and the grey dashed circle draw the temperature undulation of the thermocouple ($\Delta T'$) and the corresponding undulation centre, respectively. (d) The crosswise comparison of the rotation-induced azimuthal temperature undulations at different rotation rates.

3.1 Azimuthal temperature undulation

At a rotation rate of 1 rpm, as shown in the insets of Fig. 2a, the main peak ($t_{R\text{-}1}$ = 59.88 s) in the FFT-based MSA spectrum proves that the original (O-) GEMF spectrum is highly consistent with the actual rotation period (60 s). In addition, the direct correlation between the GEMF and the rotation could be proved by the morphology of the growth striations.[33] Specifically, considering a pulling rate of 10 mm h^{-1} and the drawdown of the liquid level, the equal-spaced rotation striation (d_R = 178.5 μm) is coincident with the GEMF fluctuation. In addition, the spectrum amplitude possesses further important details of the temperature. Since the forced convection is weak at low rotation rates, the flow pattern is simply controlled by the coupled Marangoni-buoyancy convection in the free melt surface.[43] In this case, the temperature is solely responsible for affecting GEMF, which implies that the GEMF fluctuation can be simply ascribed to the Seebeck effect. Therefore, the quantification of the temperature undulation should refer to the Seebeck EMF of the CZ-based CLN growth system, $\phi_{sbk} = \alpha_L(T_2 - T_0) + \alpha_S(T_0 - T_1)$, where $T_{0,1,2}$ are the temperatures of the growth interface, the seed crystal and the platinum crucible, respectively. Moreover, considering the stable heating system and the geometric structure of the crystal boule, when the growth interface undergoes a transient weak fluctuation, the related variations of $T_{1,2}$ can be ignored. Thus, at 1 rpm, the GEMF fluctuation can be simplified as the Seebeck variation ($\Delta\phi_{sbk}$) and ΔT_R represents the corresponding temperature undulation in the crystal rotation path (R-temp undulation),

$$\Delta\phi_{sbk} = \Delta T_R(\alpha_S - \alpha_L) \tag{3}$$

then, ΔT_R could be depicted as a function of the azimuthal angle of crystal rotation in Fig. 2a and further generalized as a pie graph in Fig. 2c (1 rpm). In the crystal rotation path, the azimuthal temperature undulation (the angle of the sighthole is $2n\pi$, where n is an integer) and evident inflection points in each lap are observed. To clarify the calculated thermal undulation, the simultaneous practical temperature variation of the eccentric rotation edge ($\Delta T'$) is shown in Fig. 2a and c, in which we can see the completely consistent tendency between the GEMF-based data and the thermocouple (ΔT_R and $\Delta T'$). Clearly, the coincidence determines the objective existence of the temperature undulation in both the azimuthal direction and growth interface. Such an undulation in the interface could be explained by the "eccentric rotation movement" of the boule. As seen in the pie graph of 1 rpm in Fig. 2c, although the growth system is well aligned before crystal growth, the unavoidable mechanical unbalance causes eccentricity, and the dissymmetric insulations further increase the distortion of the temperature field. Since the radius of the eccentric rotation edge is larger than that of the boule, the concentric area of the rotating interface should be thermally stable, but the eccentric area will sweep the "fresh melt" in each lap. This indicates that when the crystal rotates close to one direction, the melt temperature of the specific azimuthal angle will have a stronger influence on the Seebeck potential of the eccentric area as well as the whole growth interface. In this light, considering the intense air convection and thermal radiation through the sighthole of thermal insulations, the growth interface will experience a "cool region" when it rotates close to the sighthole; accordingly, the "hot region" should be located at the opposite side. The above analysis explains the measured data ($\Delta T'$) and the GEMF-based rotation temperature undulation (ΔT_R) in the azimuthal direction, as shown in Fig. 2a and c. Moreover, a sloshing motion of the three even-distributed spokes is observed (labelled in Fig. 2a and c). The back and forth motions of these spokes are driven by the locally uneven flow in the large radial temperature and the surface tension gradient.[44]

3.2 Axial temperature undulation

When the rotation system increases to medium and high rates, forced convection further complicates the growth interface drastically. As shown in the insets of Fig. 2b, regular waves are observed in the GEMF spectrum at 30 rpm. Then, the corresponding FFT result characterizes two distinct peaks for the convection and rotation GEMF ($t_{C\text{-}30}$ and $t_{R\text{-}30}$). The measured rotation peak ($t_{R\text{-}30}$ = 1.99 s) keeps with the actual rotation period (2 s) and could refer to the analysis of low rotation rate. However, the convection GEMF ($t_{C\text{-}30}$ = 23.92 s) is due to the competition between the Ekman and buoyant flow, which is consistent with the measured convection striations (d_C = 71.2 μm). In particular, in the CZ melt, the coupled convection will form and break the balloon shaped cold plume beneath the interface periodically (the "cold plume" instability).[10,45] The schematic is shown in Fig. 1a. The forced convection is an outward hot flow stemming from the crucible bottom and the meridian plane, but the natural convection is inward and flows from the crucible edge to the growth interface.[13,44,46] This implies that the enhanced forced convection could push the interference section (between forced and natural convection) away from the growth interface, *i.e.*, as the crystal rotates faster, the effect of the Marangoni-buoyancy convection on the growth interface weakens. When the rotation-induced driving force is dominant, the inward natural flow will be suppressed by the outward forced flow.[47] More vividly, comparing the three pie graphs in Fig. 2c, the R-temp undulations (ΔT_R) decrease inversely with the rotation rates, while the rotation striations become vague (compared with those shown in the insets of Fig. 2a and b). At 14 rpm, the cool spokes become weak and random (detailed discussion of 14 rpm will be presented in following page); when the rotation increases to 30 rpm, the trace of the spoke pattern disappears completely. At this time, as predicted by Li *et al.*,[43,44,47] more complex and intense flow patterns appear in the melt surface, while the GEMF spectrum indicates that the Marangoni-buoyancy convection cannot disturb the growth interface anymore.

However, the high rotation rates would induce a periodic convection, which undulates the growth interface drastically.

As seen in Fig. 2d, compared with the large and regular undulations at low rotation rates (1 and 5 rpm), the R-temp waves of the medium and high rates (14 and 30 rpm) present significant instability. This indicates that the azimuthal temperature is also strongly affected by the convection fluctuation. Furthermore, considering the high Prandtl number (Pr = 13.6) of the CLN melt, there is a strong coupling between the melt convection and the thermal field. This convection-induced temperature and growth rate fluctuations (ΔT_C, Δv) can be revealed by the variation of the supercooling and crystallization EMFs in eqn (2) and (1) together (Δv will be discussed in the next section). Then, combining the convection GEMF data at 30 rpm and a pulling rate of 10 mm h^{-1}, the corresponding supercooling degree could be depicted as a green wave curve shown in Fig. 2b. Clearly, compared with the stable melt convection at low rotation rates, in the case of high rotation rate, the supercooling curve presents a drastic convection-induced temperature undulation (C-temp undulation, ΔT_C = 1.0 °C). This may explain the inducement of the interface instability under forced convection. It should be noted that ΔT_C is the average response of the growth interface to the convection fluctuation, but the oscillatory plume should be unevenly distributed,[10] and so should the thermal field at the interface. The above discussion implies that on the issue of the temperature undulation of growth interface, there is a dilemma in choosing the rotation rate due to the natural and forced convections.

More specifically, the natural convection is an intrinsic flow and dominates the CZ melt at low rotation rates. However, at higher rates, the forced convection plays a necessary role in guaranteeing the homogenization of the crystal boule, which suppresses the component segregation and the rotation-induced temperature undulation around the growth interface. However, it triggers convection fluctuations and leaves convection striations.[9] As an inherent characteristic of the CZ melt, the basic mechanism of diverse convention and temperature fluctuations has been fully discussed by numerical simulation studies,[48,49] but the specific convection process and the corresponding thermal effects have barely been presented *in situ* in practical growth systems.

3.3 Growth rate fluctuation

Combining the FFT analysis and the relationship among the GEMF spectra, the crystallization process and supercooling degree, the interface fluctuations of both temperature and growth rate could be visualized *in situ*. A medium rotation rate of 14 rpm (which is preferred in our crystal growth system) with a pulling rate of 10 mm h^{-1} was chosen for detailed study. As shown in Fig. 3a and b, we can point out two characteristic frequencies of the convection and rotation waves in the original GEMF and MSA spectra. The frequency ($f_{\text{R-GE}}$ = 0.234 Hz) in accord with the actual rotation rate (0.233 Hz) is defined as the rotation GEMF. And the other frequency,

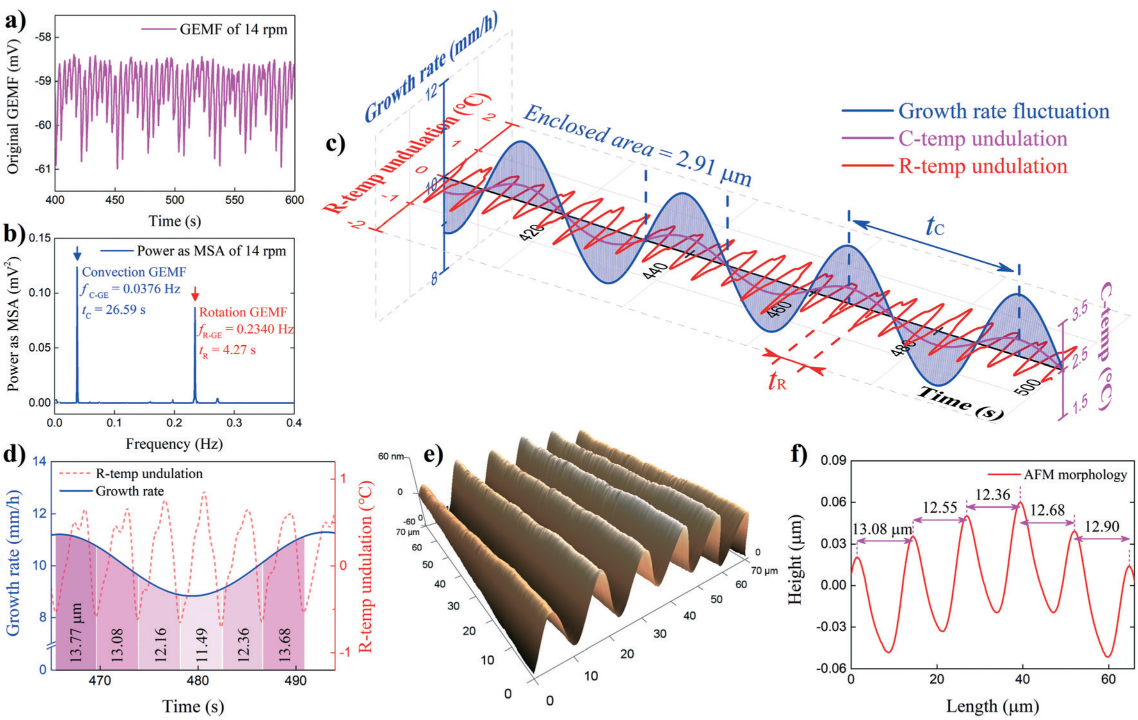

Fig. 3 (a and b) In the original GEMF and MSA spectra at 14 rpm, evident rotation and convection periods (t_R and t_C) are labelled. (c) The *in situ* visualization of growth rate, azimuthal and axial temperature (R-temp and C-temp) fluctuations. The blue enclosed (integral) area represents a convection wave height of 2.91 μm. (d) The growth rate variation and R-temp undulation in one convection period. The integral areas of growth rate variation in each rotation period are labelled in different shades of pink. (e) The fine morphology of crystal surface scanned by AFM, whose cross-section drawn (f) presents a gradient distribution of rotation striations.

defined as the convection GEMF, depicts the consequence of convection fluctuations in the growth interface. As discussed above, the rotation GEMF simply represents the R-temp undulation in the crystal rotation path, while the convection GEMF reflects both the variation of the supercooling degree and growth rate fluctuations such as flood and ebb in the axial direction.[33] Then, based on the MSA spectrum, if we extract the two characteristic frequencies from the original GEMF spectrum, the performance of the growth rate, the azimuthal temperature (R-temp) and the axial temperature (C-temp) undulations could be discussed. Specifically, the real-time growth rate fluctuations could be obtained *via* eqn (1), while the rotation- and convection-induced temperature variations refer to eqn (3) and (2). Thus, as shown in Fig. 3c, evidence that reveals the different types of interface fluctuations is visualized. We can point out the quasi-periodic temperature and growth rate fluctuations ($\Delta T_R \in (1.0, 1.7)$ °C, ΔT_C = 0.6 °C and Δv = 2.4 mm h^{-1}). Moreover, the difference between the fluctuant growth rate and the constant pulling rate represents the relative reciprocating motion between the growth interface and the free melt surface. Hence, the integral result (enclosed area = 2.91 μm) of each growth rate wave should be the "wave height" of the convection flow, which act such as sea waves striking a reef and engraving striations periodically.

3.4 Gradient striations distribution

Since a crystal pulls and rotates at constant rates, rotation striations are considered uniformly distributed. This uniformity is even used to mark the periodic laminar domain or to locate specific manual operations over the growth duration. However, as shown in Fig. 3c, based on the constant rotation period and the convection-induced quasi-periodic growth rate fluctuations, a special morphology of gradient-distributed rotation striations could be predicted. Specifically, a single convection period (t_C) is enlarged, as shown in Fig. 3d, where the wave shaped curve implies a varying growth rate in each rotation period (t_R). Therefore, the corresponding integral area represents the displacement between two rotation striations, which results in an odd regularity of gradient striation spaces. Fig. 3e and f present the high-resolution three-dimensional AFM image and cross-section drawn of the as-grown crystal boule, whose gradient peak-to-peak morphology is easily pointed out. On comparing Fig. 3d and f, our GEMF-based prediction could be confirmed by the scanned surface morphology, which vividly presents the subtle effect of the melt convection on the growth rate. More importantly, the consistency between the prediction and the actual morphology demonstrates the outstanding sensitivity and accuracy of the GEMF method.

4. Conclusions

We performed experimental studies on the GEMF spectra recorded under different rotation rates to present the effects of multiflows in a practical CZ configuration. Benefiting from GEMF, the quasi-periodic growth rate fluctuation, the axial and azimuthal temperature undulations of the growth interface are visualized *in situ*. Moreover, the observed destabilization of the spoke pattern in the free melt surface and the predicted surface morphology prove the sensitivity and accuracy of GEMF feedback. Notably, this *in situ* feedback could build a closed-loop convection control system to serve the dynamic suppression of interface fluctuation (as feedback for the ACRT, AVC and magnetic field methods, for instance), and the real-time presentation of temperature undulations offers visual guidance to optimize the symmetry of the crystal growth system. Clearly, these advantages pave a significant new approach to reveal practical melt convection instabilities and provide a strong guarantee for the development of striation-free and high-quality bulk crystals.

Conflicts of interest

There are no conflicts to declare.

Acknowledgements

This study was supported by the National Natural Science Foundation of China (NSFC) (No. 51802358, 11832019, 11372361), the National Natural Science Foundation of Guangdong Province (2018A030313321, 2017A030310426), the Guangdong Science & Technology Project (2015B090927005) and the Fundamental Research Funds for the Central Universities (17lgpy37).

References

1 C. Guguschev, J. Hidde, T. M. Gesing, M. Gogolinb and D. Klimm, *CrystEngComm*, 2018, **20**, 2868.
2 D. Junling and L. Lijun, *CrystEngComm*, 2018, **20**, 6925.
3 S. Zermout, F. Mokhtari, A. Nehari and I. Lasloudji, *CrystEngComm*, 2018, **20**, 5220.
4 H. Tian, P. Tan, X. Meng, C. Hu, G. Shi, Z. Zhou and X. Wang, *Cryst. Growth Des.*, 2016, **16**, 325.
5 E. A. Volkova, V. V. Maltsev and N. I. Leonyuk, *CrystEngComm*, 2017, **19**, 1071.
6 E. Bucchignani and D. Mansutti, *Phys. Rev. E: Stat., Nonlinear, Soft Matter Phys.*, 2004, **69**, 056319.
7 A. Klos, J. Z. Domagala and A. Bajor, *Cryst. Growth Des.*, 2008, **8**, 3253.
8 J. Nozawa, S. Uda, Y. Naradate, H. Koizum, K. Fujiwara, A. Toyotama and J. Yamanaka, *J. Phys. Chem. B*, 2013, **117**, 5289.
9 H. J. Scheel, *J. Cryst. Growth*, 2006, **287**, 214.
10 M. Teitel, D. Schwabe and A. Y. Gelfgat, *J. Cryst. Growth*, 2008, **310**, 1343.
11 R. Faiez and Y. Rezaei, *Jpn. J. Appl. Phys.*, 2016, **55**, 125602.
12 H. J. Sung, Y. J. Jung and H. Ozoe, *Int. J. Heat Mass Transfer*, 1995, **38**, 1627.
13 M. H. Tavakoli, S. Omid and E. Mohammadimanesh, *CrystEngComm*, 2011, **13**, 5088.

14 H. C. Kuhlmann and S. Albensoeder, *Phys. Rev. E: Stat., Nonlinear, Soft Matter Phys.*, 2008, 77, 036303.
15 M. T. Santos, J. C. Rojo, A. Cintas and E. Diéguez, *J. Cryst. Growth*, 1995, **156**, 413.
16 R. Teng, Q. Chang, Y. Li, B. Cui, Q. Xiao and G. Zhang, *Rare Met.*, 2017, **36**, 289.
17 A. Sheikhi, Y. L. Pouya and E. Balikci, *Cryst. Growth Des.*, 2016, **16**, 2429.
18 K. Kakimoto, H. Konishi, A. Tashiro, Y. Hashimotoa, H. Ishiia, T. Shinozakia and K. Kitamurac, *J. Electrochem. Soc.*, 2003, **150**, J17.
19 J. C. Liu, W. Q. Jie and Y. H. Zhou, *Prog. Nat. Sci.*, 1997, 7, 89.
20 W. Zhang and P. S. Halasyamani, *CrystEngComm*, 2017, **19**, 4742.
21 V. I. Strelov, E. N. Korobeynikova and V. I. Folomeev, *Cryst. Growth Des.*, 2010, **11**, 69.
22 I. Avetissov, A. Sadovskiy, S. Belov, A. Khomyakov, K. Rekunov, V. Kostikov and E. Sukhanova, *CrystEngComm*, 2013, **15**, 2213.
23 Y. Arai, K. Kinoshita, T. Tsukada, M. Kubo, K. Abe, S. Sumioka, S. Baba and Y. Inatomi, *Cryst. Growth Des.*, 2018, **18**, 3697.
24 R. Rudolph and K. Kakimoto, *MRS Bull.*, 2009, **34**, 251.
25 H. Mei, Z. Zeng, Z. Qiu, L. Li, L. Yao, H. Mizuseki and Y. Kawazoe, *Int. J. Heat Mass Transfer*, 2013, **64**, 882.
26 J. I. Choi and H. J. Sung, *Int. J. Heat Mass Transfer*, 1997, **40**, 1667.
27 M. Honarmandnia, M. H. Tavakoli and H. Sadeghi, *CrystEngComm*, 2016, **18**, 3942.
28 M. Honarmandnia, M. H. Tavakoli and H. Sadeghi, *CrystEngComm*, 2017, **19**, 576.
29 H. L. Peng, D. M. Herlach and T. Voigtmann, *Phys. Rev. Mater.*, 2017, **1**, 030401.
30 X. Kang, L. Liang, W. Song, F. Wang, Y. Sang and H. Liu, *CrystEngComm*, 2016, **18**, 8136.
31 S. Lin, C. Xiong, D. Ma, H. Li, S. Long and B. Wang, *J. Mater. Chem. C*, 2018, **6**, 10067.
32 Y. Z. Zhu, S. P. Lin, Y. Zheng, D. C. Ma and B. Wang, *J. Mater. Sci.*, 2016, **51**, 3155.
33 Y. Z. Zhu, F. Tang, X. Yang, M. Yang, D. C. Ma, X. Zhang, Y. Liu, S. P. Lin and B. Wang, *J. Cryst. Growth*, 2018, **487**, 120.
34 Y. Z. Zhu, D. C. Ma, S. W. Long, F. Tang, S. P. Lin and B. Wang, *J. Cryst. Growth*, 2017, **475**, 70.
35 H. Kimura, H. Koizumi, T. Uchida and S. Uda, *J. Cryst. Growth*, 2009, **311**, 1553.
36 H. Ozoe, K. Toh and T. Inoue, *J. Cryst. Growth*, 1991, **110**, 472.
37 C. J. Jing, N. Imaishi, S. Yasuhiro and Y. Miyazawa, *J. Cryst. Growth*, 1999, **200**, 204.
38 H. Kimura and S. Uda, *J. Cryst. Growth*, 2009, **311**, 4094.
39 A. L. Aleksandrovskii and D. P. Shumov, *Cryst. Res. Technol.*, 1990, **25**, 1239.
40 J. Nozawa, S. Iida, C. Koyama, K. Maeda, K. Fujiwara, H. Koizumi and S. Uda, *J. Cryst. Growth*, 2014, **406**, 78.
41 B. Cockayne and M. P. Gates, *J. Mater. Sci.*, 1967, **2**, 118.
42 P. Hintz and D. Schwabe, *J. Cryst. Growth*, 2001, **222**, 356.
43 W. Y. Shi, M. K. Ermakov, Y. R. Li, L. Peng and N. Imaishi, *Microgravity Sci. Technol.*, 2009, **21**, 289.
44 Y. R. Li, L. Zhang, L. Zhang and C. M. Wu, *Int. J. Heat Mass Transfer*, 2018, **117**, 835.
45 T. Munakata and I. Tanasawa, *J. Cryst. Growth*, 1990, **106**, 566.
46 S. S. Son and K. W. Yi, *J. Cryst. Growth*, 2005, **275**, e249.
47 C. M. Wu, Y. R. Li and R. J. Liao, *Int. J. Heat Mass Transfer*, 2014, **79**, 968.
48 R. Faiez and Y. Rezaei, *J. Cryst. Growth*, 2017, **457**, 72.
49 C. Stelian, T. Duffar, J. L. Santailler and I. Nicoara, *J. Cryst. Growth*, 2002, **237**, 1701.